ICARUS **130**, 387–403 (1997)
ARTICLE NO. IS975836

Broadband Submillimeter Spectroscopy of HCN, NH_3, and PH_3 in the Troposphere of Jupiter

G. R. Davis

Institute of Space and Atmospheric Studies, University of Saskatchewan, 116 Science Place, Saskatoon, Saskatchewan S7N 5E2, Canada
E-mail: G.R.Davis@usask.ca

D. A. Naylor

Department of Physics, University of Lethbridge, 4401 University Drive, Lethbridge, Alberta T1K 3M4, Canada

M. J. Griffin

Department of Physics, Queen Mary and Westfield College, Mile End Road, London E1 4NS, England

T. A. Clark

Department of Physics and Astronomy, University of Calgary, 2500 University Drive NW, Calgary, Alberta T2N 1N4, Canada

and

W. S. Holland

Joint Astronomy Centre, 660 N. A'Ohoku Place, University Park, Hilo, Hawaii 96720

Received October 20, 1995; revised June 13, 1997

We report measurements of the Jupiter brightness spectrum in the 850-μm and 1100-μm atmospheric windows with a spectral resolution of 125 MHz, obtained with a Fourier transform spectrometer on the James Clerk Maxwell Telescope. Three results were obtained. First, the predicted absorption features due to the rotational lines of HCN at 266 and 354 GHz were not detected within our error limits of less than 1%. We establish new upper limits for the HCN abundance in the jovian troposphere for five assumed abundance distributions and for two assumed NH_3 abundances. The upper limits are 1.7 to 13 times smaller than the abundance value obtained in the only reported detection of HCN in Jupiter prior to the impact of Shoemaker–Levy 9. Second, the continuum brightness temperature spectrum at 850 μm was determined and is in agreement with previous measurements, but has large error bars due to uncertainties in the photometric calibration. We estimate the ammonia abundance in the 1–2 bar region to be 1.7 times solar, but this result is tentative since scattering by NH_3 cloud particles and absorption by gaseous H_2S were neglected in our atmospheric model. Finally, the first rotational line of PH_3 at 267 GHz was not detected, a result which we demonstrate is consistent with the statistical noise level in these measurements, with current values of the spectroscopic parameters, and with phosphine measurements at other wavelengths. © 1997 Academic Press

Key Words: **abundances, atmospheres; atmospheres, composition; data reduction techniques; Jupiter; Jupiter, atmosphere; radiative transfer; spectroscopy.**

1. INTRODUCTION

Hydrogen cyanide is a known precursor in the abiotic chemical synthesis of amino acids and other organic molecules in reducing atmospheres (Ferris and Hagan 1984; Dickerson 1978; Sagan and Miller 1960). The only reported detection of HCN in Jupiter's atmosphere to date was by Tokunaga *et al.* (1981), who measured three absorption lines near 13.5 μm and inferred a mole fraction[1] of 1.8×10^{-9} in the upper troposphere, with an uncertainty of a factor of 2. Subsequent model calculations by Lellouch *et al.* (1984b) and Bézard *et al.* (1986) indicated that this abundance of tropospheric HCN should produce a series of deep, broad absorption lines throughout the jovian submm/mm spectrum.

These broad features are ideally suited to detection with a broadband spectrometer with moderate spectral resolu-

[1] Throughout this paper, we measure constituent abundances by the ratio of partial pressure to total pressure.

0019-1035/97 $25.00
Copyright © 1997 by Academic Press
All rights of reproduction in any form reserved.

tion. We report below our attempt to measure the tropospheric absorption features due to the HCN rotation lines at 266 and 354 GHz using a polarizing Fourier transform spectrometer (FTS) on the James Clerk Maxwell Telescope (JCMT). In the course of these measurements we have also determined the continuum brightness temperature in the 850-μm atmospheric window, from which we infer the NH_3 abundance between 1 and 2 bar. Finally, we have assessed the observability of the PH_3 rotation line at 267 GHz. All of the measurements reported herein predate the collision of comet Shoemaker–Levy 9.

2. MEASUREMENTS

2.1. Instrumentation

The polarizing FTS used in these measurements has evolved over several runs on the JCMT (Naylor *et al.* 1991, 1993, 1994a) and was fully described by Naylor *et al.* (1994b). The maximum spectral resolution is 125 MHz (0.004 cm^{-1}), and the spectral bandpass is defined by filters in the detector subsystem which are matched to the atmospheric windows. The polarizing FTS has two input ports and is operated in a differential mode, which is critical for the detection of weak astronomical signals in the presence of emission from the terrestrial atmosphere.

The FTS was placed at the east Nasmyth focus of the JCMT and received f/35 beams from the telescope in each input port, one of which was pointed at the center of Jupiter while the other was pointed at a neighboring region of the sky. The atmospheric emission components in each port therefore effectively cancelled within the instrument. The JCMT facility bolometric detector, UKT14 (Duncan *et al.* 1990), was placed at the FTS output port. Previous experience with this subsystem has revealed the presence of pervasive channel fringes due to parasitic Fabry–Perot effects in its internal optical system (Naylor *et al.* 1993), a feature which is irrelevant for conventional photometry, but which greatly complicates the spectroscopic calibration (Section 3.4).

2.2. Observations

The two HCN lines of interest fall into two atmospheric windows (denoted 1100 μm and 850 μm), which correspond to bandpass filters in UKT14. The 850-μm spectrum was measured during one night in 1993 May, while the 1100-μm spectrum was measured over three nights in 1994 May. The FTS was operated at its maximum resolution (125 MHz) for both runs, since the HCN absorption features at 266 and 354 GHz were predicted by Lellouch *et al.* (1984b) to have widths of ~2 GHz. The rapid scan mode was used for all measurements to minimize the effect of fluctuations in atmospheric transmittance during the scans. The scan time in this mode was ~60 s. For each run, the focal plane aperture in the detector subsystem was matched to the JCMT diffraction limit at the corresponding wavelength in order to satisfy the Jacquinot criterion for spectral resolution (Jacquinot 1960). The observing parameters and statistics for the two observing runs are listed in Table 1.

TABLE 1
Parameters and Statistics for the Observing Runs

Date	93.5.9	94.5.17/18	94.5.19/20	94.5.20/21
Filter	850 μm	1100 μm	1100 μm	1100 μm
Aperture	47 mm	65 mm	65 mm	65 mm
Half power beam width	13″	19″	19″	19″
Mean Jupiter diameter	40.8″	42.6″	42.6″	42.6″
Mars diameter	5.9″			
FTS beam separation	65″	46″	46″	46″
No. spectra, port 1	23	35	35	42
No. spectra, port 2	22	35	36	42
Mean airmass	1.144	1.349	1.266	1.467
Mean precipitable H_2O	0.61 mm	0.96 mm	2.50 mm	3.16 mm
Experimental NET	0.4 K	0.90 K	0.90 K	0.90 K
Theoretical NET (good)	0.1 K	0.05 K	0.05 K	0.05 K
Theoretical NET (poor)	0.7 K	0.15 K	0.15 K	0.16 K

Note. The theoretical noise equivalent temperature (NET) was calculated for good and poor observing conditions, as explained in the text.

It was immediately apparent from the first observations in 1993 May that the interferogram was dominated by an imbalance signal between the two input beams, which we established was due to differential spillover of the two beams around the JCMT secondary mirror. We therefore observed Jupiter in both ports of the FTS and removed the imbalance signal by differencing the spectra during data analysis (Section 3.3). This procedure was followed in both runs, although the imbalance signal was much smaller in 1994 May due to the reduced angular separation of the two input beams on that occasion. The observing cycle consisted of five spectra with Jupiter in port 1, followed by five spectra with Jupiter in port 2, and was repeated throughout the observing shift. The numbers of scans in each run with Jupiter in each port are listed in Table 1.

3. ANALYSIS

3.1. Data Processing

Some of the recorded interferograms contained obvious transients caused by cosmic rays and/or electromagnetic interference. These were manually removed using an interactive graphical computer program written in Interactive Data Language (Research Systems Inc., Boulder, Colorado). Fourier transformation of the edited interferograms followed the method described by Naylor *et al.* (1994b). Since the optical elements in the spectrometer and detector produced negligible dispersion over the narrow range of interest, a linear phase correction was determined by weighting phase values obtained from the Fourier transform of a short double-sided interferogram by the amplitude of the corresponding spectrum, and was applied to each interferogram individually before Fourier transformation.

3.2. *Atmospheric Transmittance*

The raw spectra were not directly averaged because of temporal variations in the atmospheric transmittance, which arose from two sources: the slowly varying elevation of the target as the Earth rotated, and the variable water vapor content of the terrestrial atmosphere. For the present observations, these variations occur on three relevant time scales: first, variations over ~2 h within a single observing shift; second, variations between different parts of an observing shift (Mars was the intended calibrator for these measurements, but in 1993 May Mars was only available earlier in the shift than Jupiter and the two sets of measurements were therefore carried out sequentially); and third, variations between different nights in an observing run (the 1100-μm measurements in 1994 May were spread over three nights on which the atmospheric conditions were significantly different). For these reasons, we required a model of the atmospheric transmittance variations in order to compare spectra taken under different observing conditions. We present in this section our correction algorithm for variable atmospheric transmittance.

The two relevant variables are the airmass a and the atmospheric water vapour content, which is highly variable on a wide range of temporal and spatial scales. While the airmass is always well known, varies smoothly with time and is recorded in the telescope pointing archive, the atmospheric H_2O is less well defined. In general, the H_2O concentration along the line of sight may vary in an unknown manner with the meteorological conditions, giving rise to a large number of degrees of freedom. We choose to simplify the problem by parameterising the atmospheric transmittance in terms of the total zenith H_2O column amount, which we characterise by the precipitable water vapour w.

In order to characterise the dependence of the atmospheric transmittance on the precipitable H_2O, we ran the atmospheric spectral synthesis program FASCOD2 (Clough *et al.* 1986) for w values of 0.5, 1, 2, 3 and 4 mm. The vertical pressure and temperature distributions were taken from the U.S. Standard Atmosphere (National Oceanic and Atmospheric Administration 1976) for the appropriate latitude and altitude (20°N, 4.2 km). The atmospheric absorbers included in the calculation were H_2O, O_3, and O_2, since these constituents dominate the opacity at these wavelengths. The H_2O mixing ratio was multiplied by a constant factor in each run corresponding to the selected precipitable amount. The spectral line parameters for all gases were taken from the 1986 HITRAN compilation (Rothman *et al.* 1987); the program also includes the continuum absorption by H_2O (Clough *et al.* 1989), which is poorly characterized at these wavelengths (Davis 1993). The frequency resolution was set to 30 MHz in order to adequately sample the spectral resolution element of the FTS. Although FASCOD2 has been extensively verified against measured atmospheric spectra at other wavelengths, we note that the submillimeter atmospheric transmittance spectrum above Mauna Kea has never been measured at the resolution of the FTS. We hope to carry out such an experiment in the near future.

At each frequency in the calculation, the zenith opacity calculated by FASCOD2 was linear in precipitable H_2O (e.g., Fig. 1),

$$\tau_z(\nu) = \tau_0(\nu) + \tau_1(\nu)w, \tag{1}$$

where τ_1 is the opacity per unit of precipitable H_2O and τ_0 is the opacity due to all other absorbing gases. These coefficients were determined by linear least-squares fits at each frequency and stored for future use. The total opacity in the line of sight is then given by

$$\tau_{LOS}(\nu) = \tau_z(\nu)a. \tag{2}$$

The precipitable H_2O was monitored during these runs by a 225-GHz radiometer on the adjacent Caltech Submillimeter Observatory (CSO). The zenith opacity measured by this device τ_{CSO} was recorded and the precipitable H_2O was determined by inverting Eq. (1) at the corresponding frequency (Fig. 1):

$$w = 20(\tau_{CSO} - 0.016)\ \text{mm}. \tag{3}$$

Equations (1) through (3) provide a simple and fast method for calculating the atmospheric transmittance spectrum for any combination of a and w. There are, however, several uncertainties associated with use of the CSO radiometer as a monitor of the precipitable H_2O. First, since its temporal resolution is approximately 20 min, any H_2O fluctuations on faster time scales are not adequately sampled; it is well known that rapid humidity fluctuations do occur in association with atmospheric microstructure, which are potentially significant since the FTS scan time is only 60 s. Second, the radiometer operates by performing elevation scans at a fixed azimuth, which in general does not correspond with the azimuth of the observations and does not sample spatial variations along the line of sight. Finally, since the absolute accuracy of the radiometer is uncertain, the sensitivity to calibration errors must be taken into account (Section 5.1). Nevertheless, the CSO radiometer

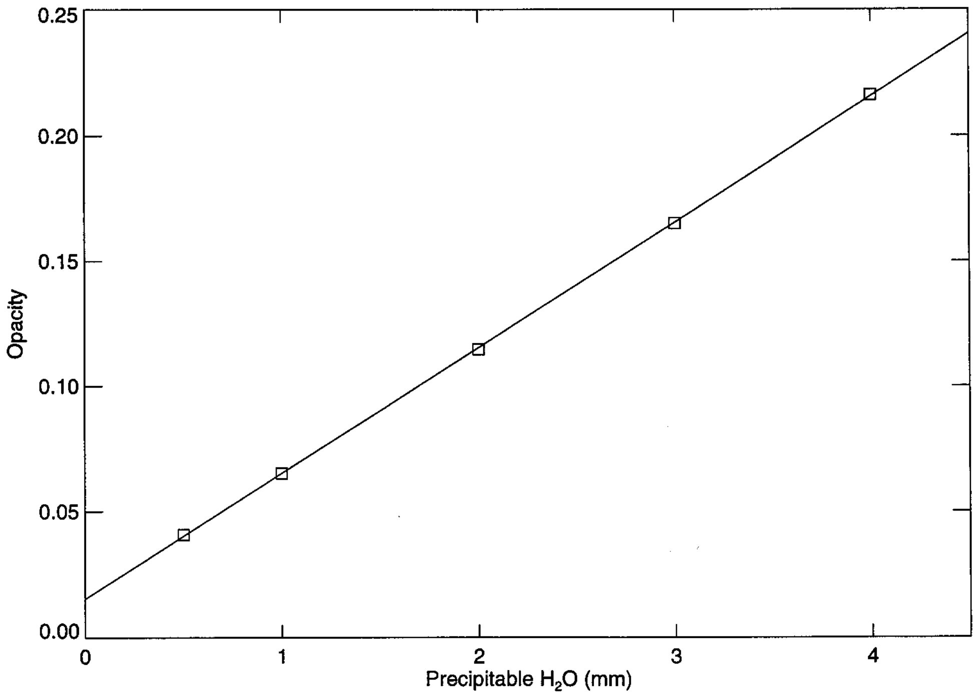

FIG. 1. Atmospheric opacity at 225 GHz. The squares denote points calculated using FASCOD2. The fitted straight line represents our calibration of the CSO radiometer. Similar fits were carried out at all frequencies in the spectral synthesis.

is the best monitor of atmospheric H_2O currently available, and we demonstrate below that the transmittance parameterization presented here works well in spite of these difficulties.

To account for variations in atmospheric transmittance during an observing shift, each spectrum was corrected to the shift-averaged transmittance by multiplication by the factor

$$\frac{\exp[-\tau_{\mathrm{LOS}}(\nu, \bar{a}, \bar{w})]}{\exp[-\tau_{\mathrm{LOS}}(\nu, a_i, w_i)]}, \tag{4}$$

where $\bar{a}$ and $\bar{w}$ are the mean values of airmass and precipitable H_2O during the shift (Table 1) and a_i and w_i are the values corresponding to the individual spectrum. The opacity spectra were calculated using Eqs. (1) and (2). As an example of this correction technique, the variations in a and w during the shift on 1994 May 19/20 are shown in Fig. 2. The airmass rose slowly as Jupiter set, while the precipitable H_2O varied between 2.2 mm and 2.7 mm (poor observing conditions). The coarse temporal resolution of the CSO radiometer is evident. As a measure of the first-order temporal trend in the measured spectra, a sequential scan number was assigned to each spectrum and the slopes of each spectral point against the scan number were determined. These slopes, determined before and after correction, are shown in Fig. 3. The overall negative slope before correction is expected since both airmass and precipitable H_2O increased during the shift. It is evident that this correction algorithm effectively removes the systematic downward trend and therefore also reduces the rms noise, despite the uncertainties associated with use of the CSO radiometer as a monitor of precipitable H_2O.

3.3. Average Spectra

The spectra obtained with Jupiter in each input port of the FTS were averaged separately for each observing shift. The internal error was characterized by the statistical error in the mean. The port-averaged spectra were then differenced to eliminate the imbalance signal between the ports (Section 2.2). The average Jupiter spectra obtained by this procedure are shown in Fig. 4. These spectra contain the combined effects of jovian emission, atmospheric transmittance, and the optical transmittances of the spectrometer and detector; the overall shapes are defined by the bandpass filters in the detector subsystem.

We have previously demonstrated excellent agreement between experimental noise levels obtained with the FTS when viewing the Sun and theoretical calculations based on the noise characteristics of UKT14 when used for conventional photometry on the JCMT (Naylor *et al.* 1993). This calculation has been repeated for the present case, and the experimental and theoretical noise equivalent temperatures (NETs) are listed in Table 1. The theoretical

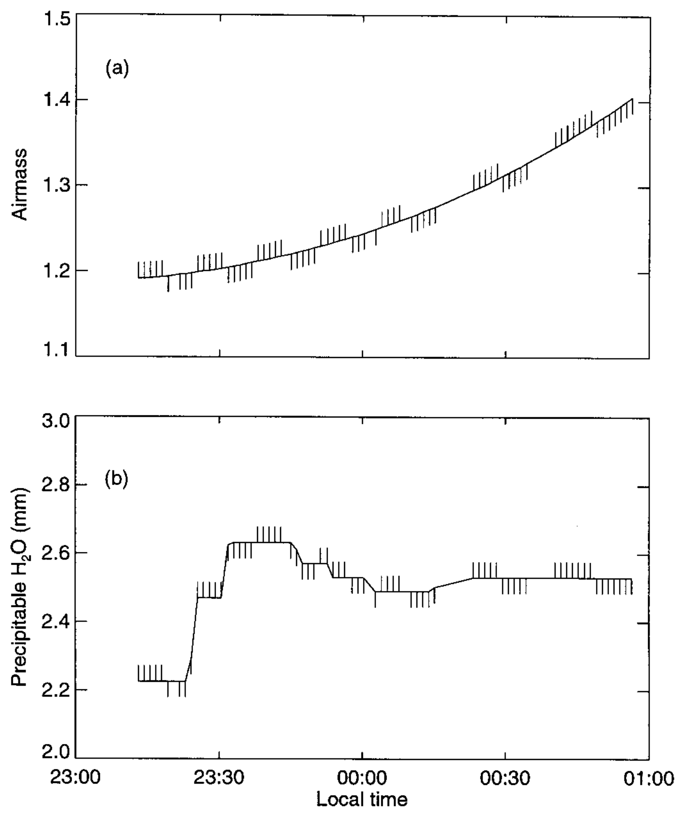

FIG. 2. Variation of (a) airmass and (b) precipitable H_2O during the shift on 1994 May 19/20. The vertical ticks represent the times of FTS scans: up for Jupiter in port 1 and down for Jupiter in port 2. The temporal resolution of the CSO radiometer is 20 minutes, while the FTS scan time is 1 minute.

NET was calculated using the photometric noise equivalent flux densities, including all telescope efficiency terms, obtained with UKT14 for both good and poor observing conditions (Matthews 1995); when combined with the efficiency of the FTS and the total integration time, Parseval's theorem yields the temperature error per spectral element. The experimental noise in the Jupiter measurements is within the expected range at 850 μm, but is clearly much higher than calculated at 1100 μm due to sky noise which is not completely removed by the transmittance correction scheme in Section 3.2. This result demonstrates the importance of atmospheric stability, which is not necessarily correlated with the absolute opacity value, when averaging over large data sets.

3.4. Calibration

In common with conventional submm/mm photometry, we had originally intended to use Mars as a calibration target. Its brightness and its tenuous atmosphere make Mars the best continuum calibrator available in this spectral region, despite the uncertainties discussed by Griffin *et al.* (1986) and by Griffin and Orton (1993). In 1993 May, a set of 59 interferograms was taken on Mars during a 2-h period immediately preceding the Jupiter measurements, and was analyzed by identical procedures. The average Jupiter and Mars spectra are shown in Fig. 5.

The Jupiter and Mars spectra are dissimilar, despite the fact that both planets are bright continuum sources. We attribute the discrepancy to channel fringes produced by parasitic Fabry–Perot effects between parallel optical surfaces in the detector subsystem, a feature which we have identified and documented in previous measurements (Naylor *et al.* 1993). Since the two planets in this case have different sizes, however, they couple to the telescope differently: Mars is smaller than the telescope field of view, while Jupiter overfills it (Table 1). Their beams therefore follow different paths through the detector optics, resulting in different fringe patterns in the two spectra. This interpretation is supported by the solar spectrum which is also shown in Fig. 5: since Jupiter and the Sun both fill the telescope field of view, their fringe patterns are well correlated. A similar, albeit smaller, effect was observed in Nep-

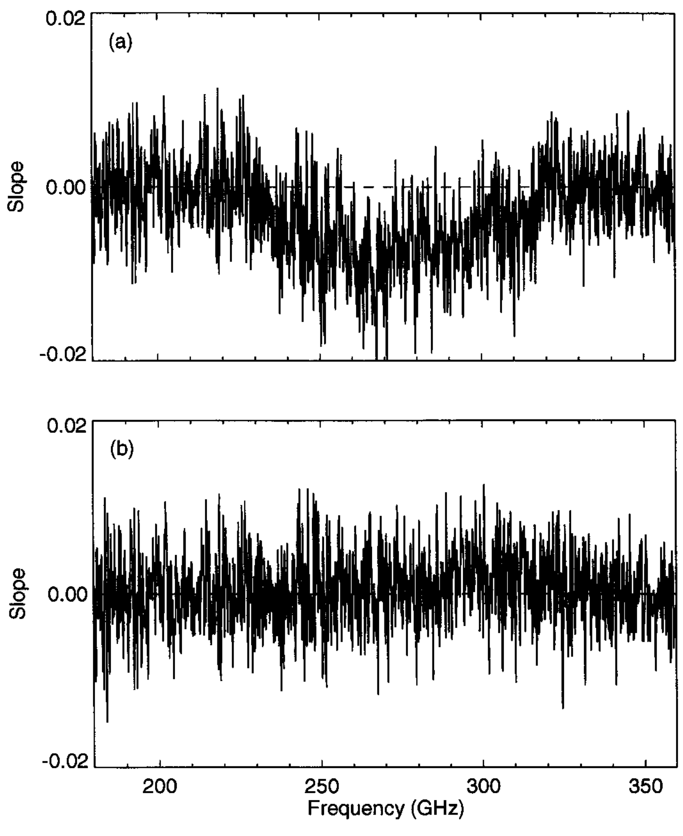

FIG. 3. Slope of each spectral point against sequential scan number for the complete set of port 2 spectra during the shift on 1994 May 19/20, (a) before and (b) after correction for variable atmospheric transmittance. The correction algorithm has reduced the average slope to near zero.

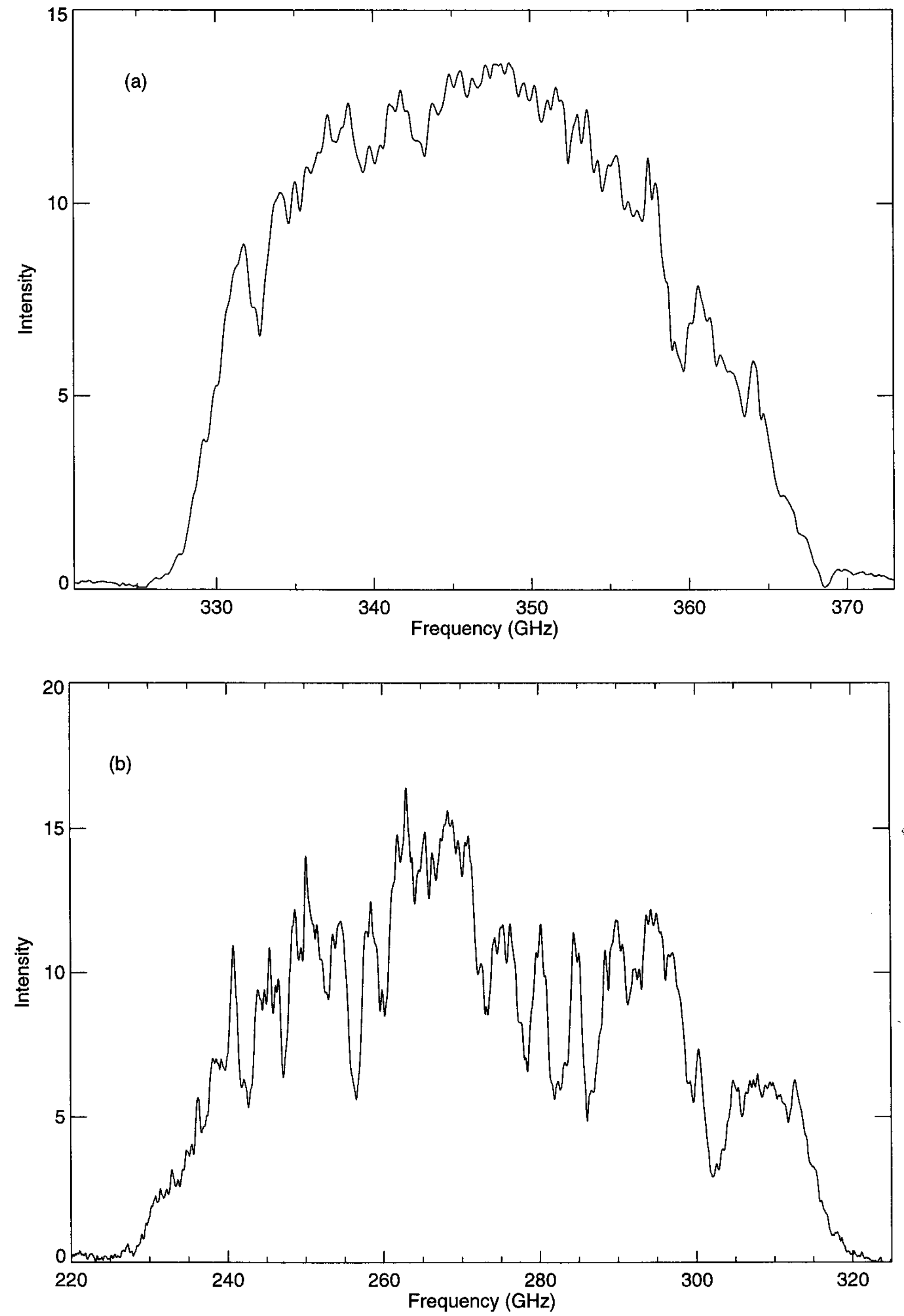

FIG. 4. Average jovian spectra: (a) 850-μm window, (b) 1100-μm window. The ordinate scale is arbitrary since these spectra are uncalibrated.

tune and Uranus spectra obtained in a previous run (Naylor *et al.* 1994a).

Channel fringes are extremely difficult to remove from the interferograms at these wavelengths (Naylor *et al.* 1988) and can only be reliably eliminated by ratioing against a calibration spectrum with an identical fringe pattern. The dependence on source size, however, requires either that the calibration target be of the same angular size as the primary source or that they both overfill the telescope field of view. For the Jupiter measurements reported here, this requirement can only be met by using either the Sun or the Moon as a calibrator, and since suitable spectra of the

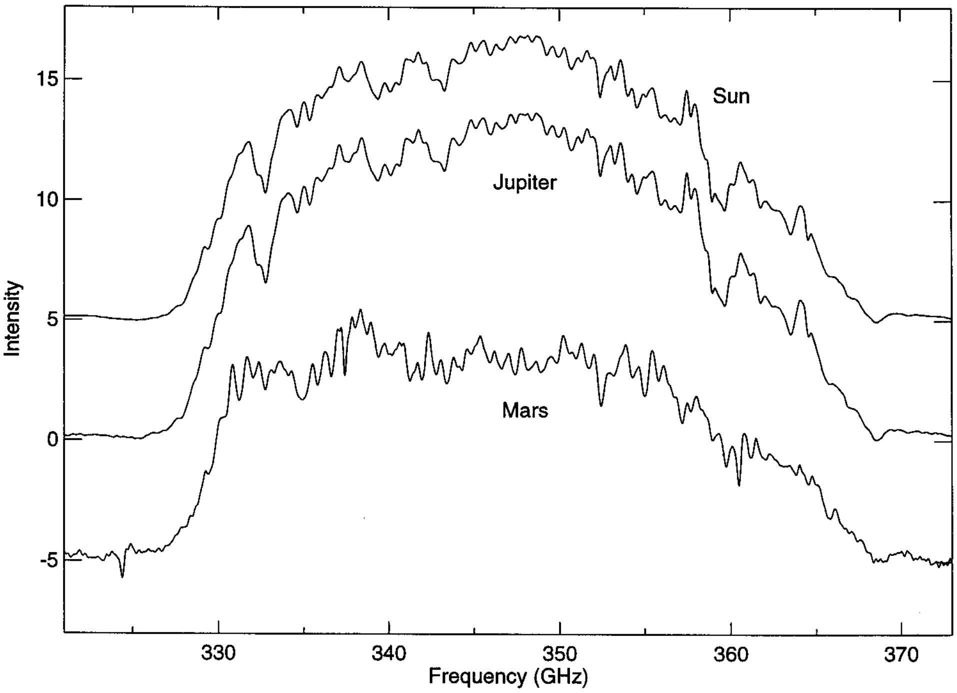

FIG. 5. Measured spectra of Jupiter, the Sun, and Mars. The solar and martian spectra have been normalized to the same height as the jovian spectrum and offset for clarity. The ordinate scale is arbitrary since these spectra are uncalibrated. The channel fringes are well matched for the jovian and solar spectra, but poorly matched for the martian spectrum.

Sun were acquired during the same observing runs as part of a search for solar H and Mg recombination lines (Clark *et al.* 1994), the Jupiter spectra were calibrated against the Sun. Although this unconventional procedure introduced a new set of uncertainties into the calibration, we demonstrate below that a reliable flux calibration was nevertheless obtained. We plan to eliminate the channel fringe problem for future measurements with a new ^3He dual polarization detector system featuring an optical design which has been carefully optimized for broadband spectroscopy.

Four suitable spectra of the Sun were obtained on the morning of 1993 May 10 (10 hours after the Jupiter measurements). Since the extended size of the Sun makes differential operation impossible, the FTS was converted to single-beam mode for the solar measurements by placing a constant-temperature target in one of the input ports. Solar and background spectra were recorded sequentially and were differenced at the data analysis stage to remove the atmospheric emission term, which was ~10% of the solar component. The port imbalance signal was negligible with respect to the solar signal and was not removed. The data analysis was otherwise identical to that described above for Jupiter. The average solar spectrum obtained in this manner is shown in Fig. 5.

The atmospheric transmittance algorithm described in Section 3.2 was employed a second time to correct the jovian and solar average spectra to the median values of airmass and precipitable H_2O. The H_2O component of this correction was small since the w values were similar despite being 10 h apart (0.612 mm for Jupiter, 0.64 mm for the Sun). The ratio of the corrected spectra is shown in Fig. 6. The complete cancellation of the telluric features which pervade the two individual spectra demonstrates both the linearity of the detector system over the large dynamic range (Section 5.1) and the accuracy of the atmospheric transmittance correction scheme used in the analysis; the small ripples which remain in this ratio are attributed to residual channel fringes which were not completely removed by calibration against the Sun. The statistical error in the Jupiter : Sun ratio, averaged over the frequency range in Fig. 6, is 0.35%.

The 1994 May data were calibrated in a similar manner. Two solar spectra were recorded in single-beam mode on the morning of 1994 May 21. In view of the high solar temperature and the inferior atmospheric conditions during this run, the signal-to-noise ratio for these two spectra was comparable to that obtained by averaging the measured Jupiter spectra over an entire shift. Background spectra were unfortunately not recorded during this run and it was therefore impossible to remove the atmospheric emission contribution. The atmospheric transmittance algorithm described in Section 3.2 was employed a second

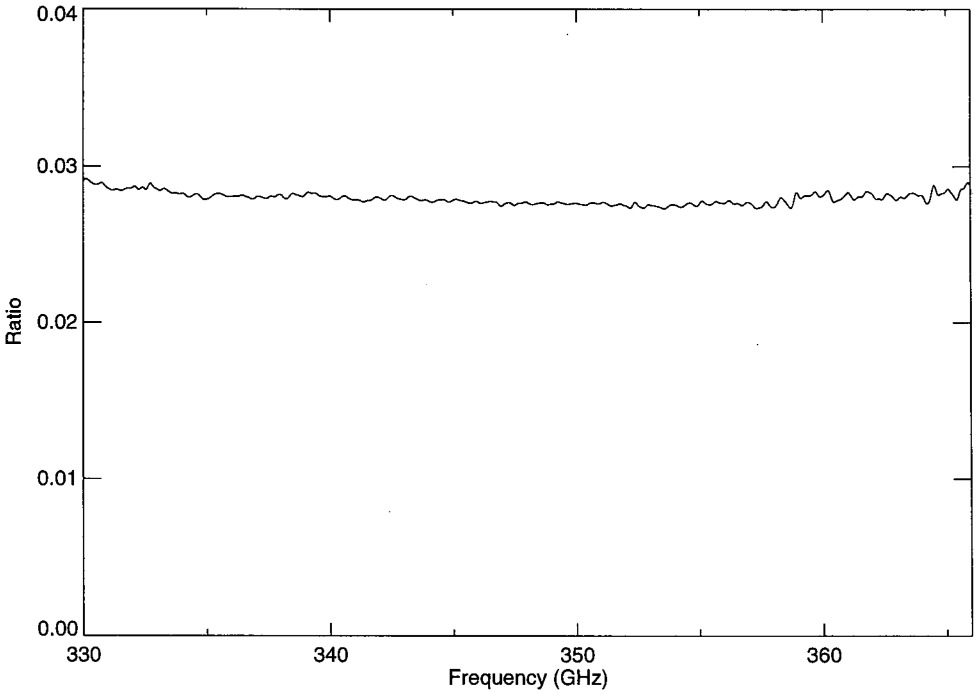

FIG. 6. Measured Jupiter : Sun ratio, 850-μm window.

time to correct the average solar spectrum to the airmass and precipitable H_2O corresponding to each of the three Jupiter shifts. The Jupiter : Sun ratio was calculated separately for each shift and the three ratios were then averaged. The average Jupiter : Sun ratio is shown in Fig. 7; the statistical error in the ratio, averaged over the frequency range in Fig. 7, is 1.3%.

4. RADIATIVE TRANSFER MODEL

A radiative transfer model of the jovian atmosphere was developed for comparison with the measured spectra. Since the telescope was pointed at the center of the resolved jovian disk for these measurements, a plane parallel representation of the atmosphere was adopted; limb darkening effects were tested and found to be negligible due to the rapid falloff of the JCMT beam profile. The atmosphere was divided into 10 layers per pressure decade and the brightness temperature spectrum was calculated according to the standard equation (Hanel *et al.* 1992)

$$T_B(\nu) = \sum_i T_i[1 - e^{-\tau_i(\nu)}]e^{-\tau_i^*(\nu)}, \qquad (5)$$

where T_i is the temperature of layer i, $\tau_i(\nu)$ is the incremental opacity of layer i, and $\tau_i^*(\nu)$ is the cumulative opacity from layer i to the top of the atmosphere. The atmosphere was assumed to be in both hydrostatic and local thermodynamic equilibria, and the Planck function was replaced by temperature in the Rayleigh–Jeans limit.

The JCMT field of view is nevertheless sufficiently large that it covers a range of jovian belts and zones. We therefore used the whole-disk temperature profile derived by Bézard *et al.* (1983) from Voyager measurements. The measured profile was extrapolated by these authors to a depth of 6.4 bar, and was further extrapolated by us to 20 bar for these calculations. The temperature range in this final extrapolation was 287–400 K, which permitted a number of simplifications. First, a dry adiabat was adopted since no species are in condensed form at these temperatures. The extrapolation therefore followed the simple equation

$$\frac{d \ln T}{d \ln p} = \frac{R}{C_p}, \qquad (6)$$

where R is the gas constant and C_p is the weighted mean of the H_2 and He specific heats. The mole fraction of H_2 was taken to be 0.897 (Gautier *et al.* 1981). Second, the specific heat of H_2 over this temperature range is independent of any assumptions concerning the ortho : para population ratio (Wallace 1980). Finally, the specific heat of H_2 is approximately constant over this temperature range. The resulting temperature profile is shown in Fig. 8.

The primary opacity mechanisms in this spectral region

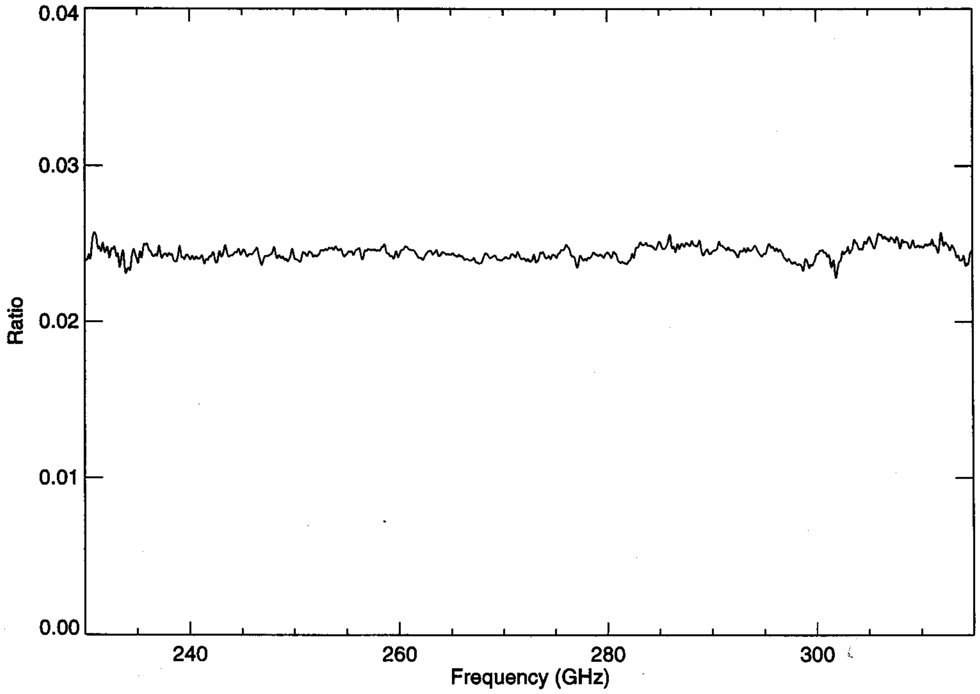

FIG. 7. Measured Jupiter : Sun ratio, 1100-μm window.

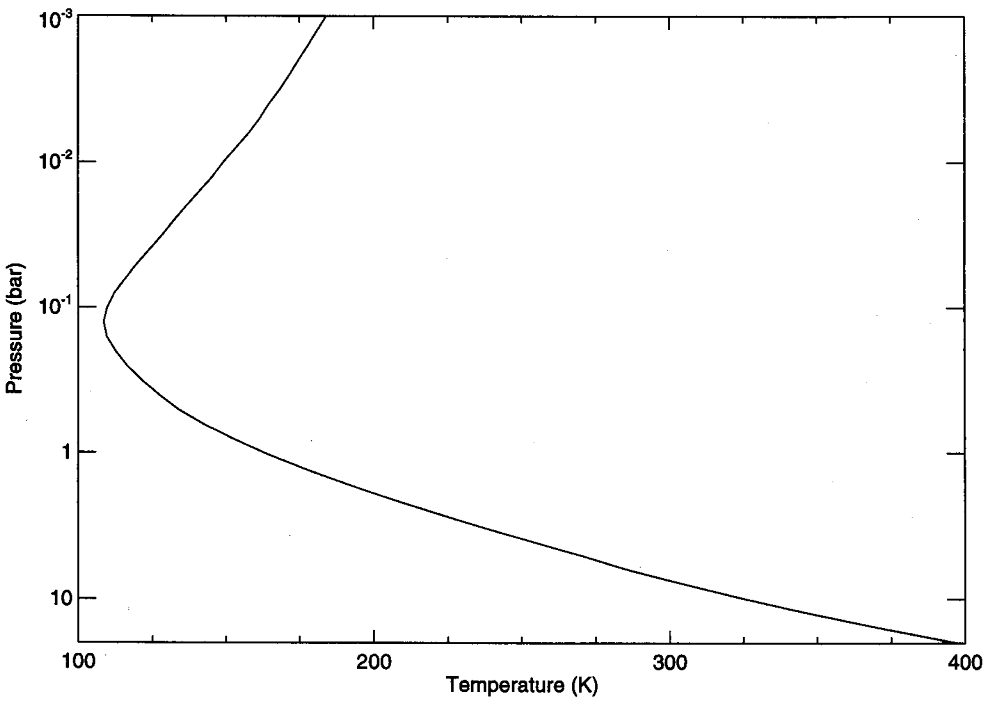

FIG. 8. Jupiter whole-disk temperature profile, adopted and extrapolated from Bézard *et al.* (1983).

are collision-induced absorption by H_2 molecules and molecular absorption by NH_3 molecules. Spectral features due to hydrogen cyanide and phosphine (PH_3) are also predicted to be present (Bézard *et al.* 1986; Lellouch *et al.* 1984b). The vertical abundance distributions of these constituents are discussed in Section 5.

The opacity due to H_2–H_2 collisions arises from a quadrupole-induced dipole interaction and was modelled following the parameterization of Dore *et al.* (1983). Only the translational component was included since the resonance terms are negligible at these wavelengths. The opacity due to H_2–He collisions, on the other hand, arises primarily from an electron overlap interaction and was modelled following the parameterization of Cohen *et al.* (1982). The isotropic overlap component dominates the opacity at these wavelengths and the anisotropic overlap and quadrupole terms were therefore not included.

Ammonia contributes the dominant opacity in this spectral region, due to the inversion band centred at 23.7 GHz and the first rotational line at 570 GHz. The frequency, intensity, and lower state energy parameters for the 128 inversion lines were taken from the 1992 GEISA compilation (Husson *et al.* 1992). The Ben-Reuven line shape (Ben-Reuven 1966) was used for the individual inversion lines, following recent measurements at mm and cm wavelengths in simulated jovian atmospheres (Joiner and Steffes 1991; Steffes and Jenkins 1987). The line width and coupling parameters were taken from Berge and Gulkis (1976). Parameters for the rotational line were obtained from the 1992 HITRAN compilation (Rothman *et al.* 1992). The Van Vleck–Weisskopf line shape was used, with a H_2-broadened width of 2.25 GHz (Varanasi 1972) and a H_2 : He broadening ratio of 3 (Berge and Gulkis 1976).

Only the $J = 4 \rightarrow 3$ HCN line at 354.5 GHz was considered in this analysis. The line parameters were obtained from the 1992 HITRAN compilation (Rothman *et al.* 1992). The Lorentz line shape was used, with the H_2- and He-broadened widths and temperature coefficients taken from the calculations of Rohart *et al.* (1987). Finally, the parameters for the $J = 1 \rightarrow 0$ PH_3 line at 266.9 GHz were taken from the JPL line catalogue (Pickett *et al.*, 1995). The Lorentz line shape was used, with the H_2-broadened width taken from the measurements by Pickett *et al.* (1981).

5. RESULTS AND DISCUSSION

5.1. Continuum Brightness Temperature

The continuum brightness temperature for Jupiter in the 850-μm atmospheric window was derived by multiplying the Jupiter : Sun ratio (Fig. 6) by the solar temperature. The latter quantity was taken as 5900 ± 500 K from the model of Avrett (Falchi *et al.* 1994). The 1100-μm measurements were not converted to temperature since background spectra were not recorded and the atmospheric emission contribution could not be removed from the solar spectra.

Although both Jupiter and the Sun overfill the telescope field of view and produce well-matched channel fringe patterns, they nevertheless couple to the telescope slightly differently because the JCMT beam profile has an extended diffraction pedestal due to surface roughness in the individual panels which compose the primary mirror. This effect was well documented by Clark *et al.* (1992), who measured the extended beam patterns at 350 and 450 μm using the Sun as a source. In order to make use of these results, which are unaffected by occasional adjustments to the JCMT dish to improve the surface accuracy, we extrapolated these measurements to 850 μm using the Ruze model (1966), with the result that the portion of the beam profile outside Jupiter's diameter contributes 10.9% of the total energy. In our measurements, the Sun filled this extended pedestal, resulting in an enhanced solar spectrum, and we have therefore increased the Jupiter brightness temperature by this same factor.

A further correction is required to account for differences in detector responsivity when viewing Jupiter and the Sun because of the different flux levels of these two objects (a factor of approximately 30). It is well known that bolometric detectors can respond nonlinearly to changes in power loading (Griffin and Holland 1988), particularly for new-generation bolometers operating at temperatures around 0.1 K (Holland *et al.* 1996). To investigate the extent of this problem for the UKT14 bolometer used in these measurements, we have developed a model of the normalized responsivity as a function of source flux per beam. The model is similar to that presented by Griffin and Holland and is based on empirical data at a wavelength of 850 μm. It includes the effects of atmospheric transmittance, beam coupling to the telescope, and FTS efficiency, all of which significantly reduce the power loading contrast on the detector. The result of this calculation is that the reduction in responsivity under solar loading is only 1.1%, and we have therefore reduced the jovian brightness temperature by this same factor. The highly linear response of the bolometer over this flux range is due primarily to the relatively high operating temperature (0.36 K) and the high thermal conductance between the bolometer and the low-temperature heat sink (Duncan *et al.* 1990).

The resultant Jupiter brightness temperature spectrum is shown in Fig. 9. Various sources of systematic error have been considered in order to estimate the uncertainty in this spectrum. First, the sensitivity of the brightness temperature to the calibration accuracy of the CSO radiometer (Section 3.2) was evaluated by direct calculation: for an opacity measurement error of 0.01 (~20% of the absolute opacity value), a temperature error of only 1% was obtained. This sensitivity is small because of the ratiometric nature of the transmittance correction (Eq. (4)) and be-

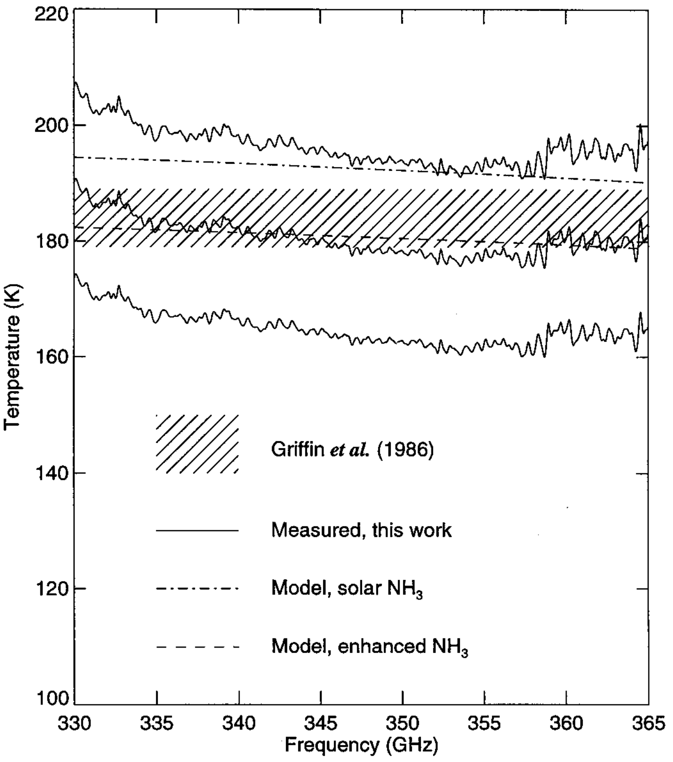

FIG. 9. Jupiter continuum brightness temperature, 850-μm window. The three solid curves represent the measured brightness temperature spectrum and the error envelopes. The shaded region represents the photometric measurement by Griffin *et al.* (1986), compensated for limb darkening, centered at 337 GHz. The broken curves represent two model calculations, for a solar ammonia abundance and for an enhanced ammonia abundance (1.7 $\times$ solar).

cause of the stable atmospheric conditions during the run in 1993 May (Section 3.4). Second, the sensitivity of the brightness temperature to the H_2O absorption model in FASCOD2 (Section 3.2) was evaluated by repeating the analysis with the H_2O continuum component completely removed from the calculation. The temperature error in this case was less than 10^{-5}, for the same two reasons. Third, we attribute an uncertainty of $\pm 2\%$ to the beam coupling factor discussed above. Finally, there is a 9% uncertainty in the solar temperature which completely dominates the error budget, a consequence of using the Sun as a calibrator (Section 3.4). The error envelope corresponding to this uncertainty is plotted in Fig. 9.

The brightness temperature of Jupiter in this atmospheric window was measured by Griffin *et al.* (1986) using conventional photometry. They obtained a temperature of 174 $\pm$ 5 K with a filter width of 150 GHz, centered at an effective frequency of 337 GHz. They also used a 65″ beam, and their measurement therefore included limb darkening effects which were negligible in the present case since the planetary disk was resolved by the JCMT beam. We have used a spherical representation of the planet in conjunction with our atmospheric model to correct the Griffin *et al.* measurement for limb darkening. The corrected brightness temperature for the central 13″ of the disk is 184 $\pm$ 5 K, which is in excellent agreement with our result (Fig. 9).

Two model calculations of the brightness temperature spectrum are also shown in Fig. 9. In the dot–dash curve, the ammonia abundance is assumed to be uniform and equal to the solar value (mole fraction 1.9 $\times$ 10^{-4}) in the deep atmosphere, and constrained by saturation at higher levels (Fig. 10). This model is within the error envelope of our measurement. Additional opacity, however, would clearly improve the agreement with our spectrum and with the Griffin *et al.* photometric measurement. We consider below various possible sources of additional opacity in the jovian atmosphere.

One possibility is an enhanced ammonia aboundance in the 1–2 bar region where the contribution function peaks (Fig. 11). The dashed curve in Fig. 9 was calculated for a distribution which was again uniform in the lower troposphere and constrained by saturation in the upper troposphere, but in which the well-mixed value was enhanced over solar by a factor of 1.7 (mole fraction 3.2 $\times$ 10^{-4}; Fig. 10). This model fits the measured spectrum extremely well and we regard this as our best-fit NH_3 abundance. Supersolar ammonia abundances at pressures greater than 2 bar have been suggested by Marten *et al.* (1980), by dePater and Massie (1985), and by Carlson *et al.* (1993); the latter two authors, however, also reported depletions to subsolar abundances between 1 and 2 bar, exactly the level at which our contribution functions peak (Fig. 11). Such a depletion is inconsistent with our measurements unless other sources of opacity are invoked.

A second possible source of opacity is absorption and/or scattering by particulates, since the NH_3 emission peaks below the NH_3 ice cloud at 0.8 bar (Fig. 11). Photometric measurements by Griffin *et al.* (1986) at shorter wavelengths, when compared with a range of NH_3 cloud scattering models, indicated the presence of particles with mode radius between 30 and 100 μm, which would produce a temperature reduction of up to ~7 K at 850 μm.

A third possibility, which was originally proposed by Bézard *et al.* (1983) and was further considered by Griffin *et al.* (1986) and Joiner *et al.* (1992), is absorption by H_2S. Bézard *et al.* calculated the jovian submm/mm spectrum for three different H_2S profiles. They showed that the H_2S opacity would be small if thermochemical equilibrium with the NH_4SH cloud particles was established at all levels, but also that if the equilibration time were substantially longer than the vertical mixing time so that condensation losses are negligible, the enhanced H_2S abundance in the upper troposphere would reduce the brightness temperature at 850 μm by ~10 K. Such an enhancement should produce observable absorption features in these windows,

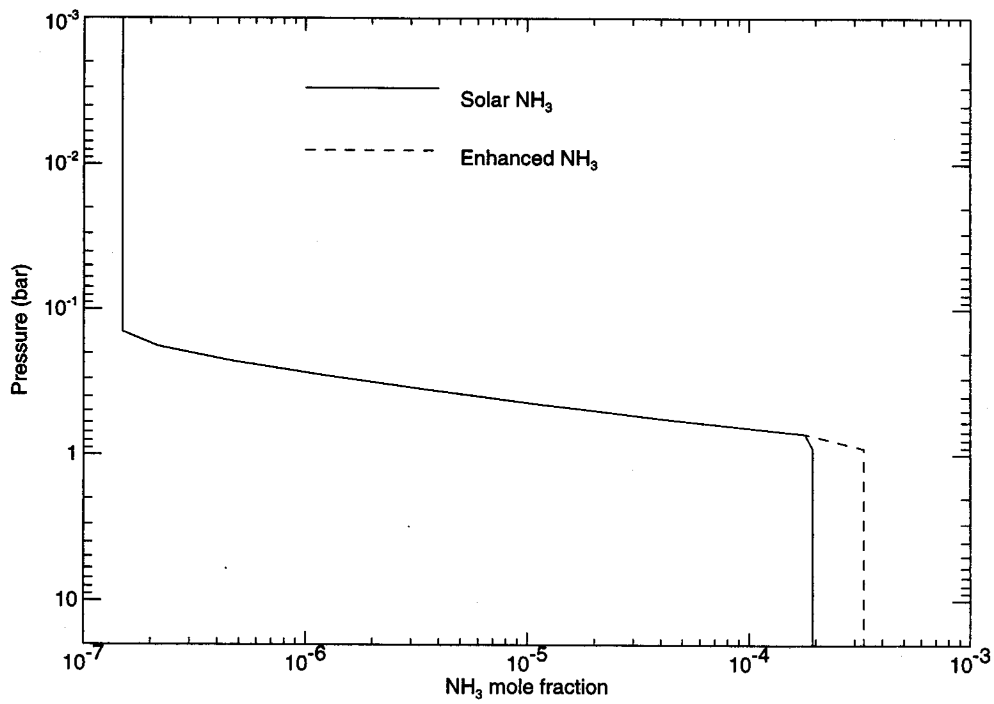

FIG. 10. Two NH_3 abundance distributions considered in the text. Both are constrained by saturation in the cloud layer. The solid curve represents a solar abundance in the lower troposphere, and the broken curve represents an enhanced abundance (1.7 × solar).

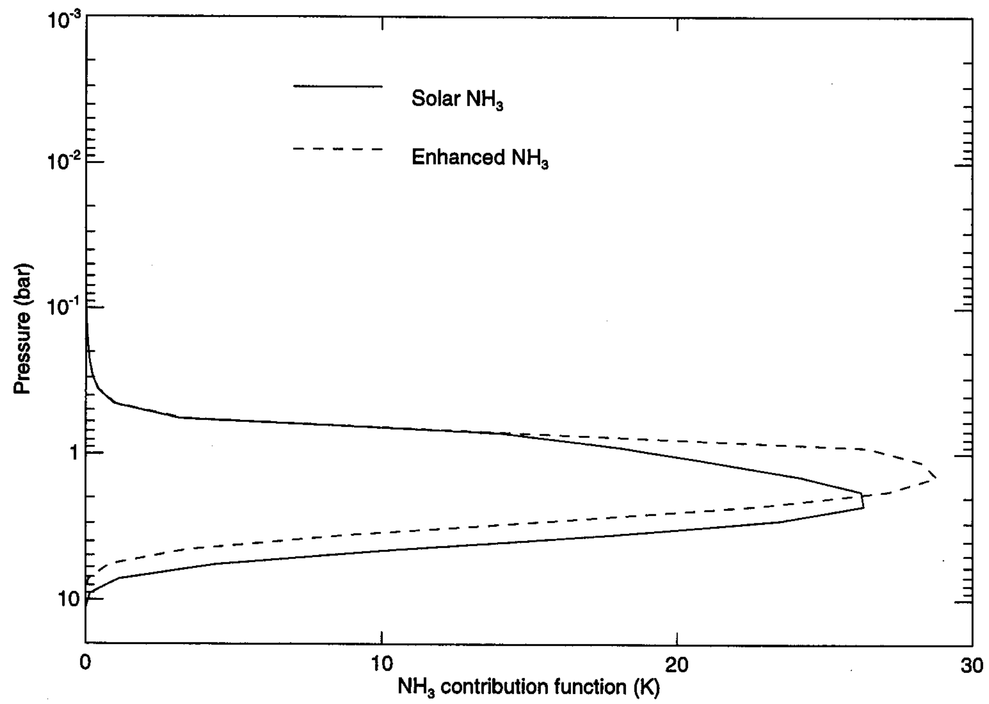

FIG. 11. The NH_3 contribution functions for the two abundance distributions. The solid curve represents the solar abundance model, and the broken curve represents the enhanced abundance (1.7 × solar) model.

however, and since the strong H_2S line at 300.5 GHz was not detected (Fig. 7), this possibility seems unlikely; the nondetection is entirely consistent with Bézard's proposed thermochemical equilibrium profile.

Clearly, the large uncertainty in our measurement prevents us from drawing any quantitative conclusion regarding even the need for additional opacity, let alone its magnitude and origin. Nevertheless we have demonstrated the potential of broadband spectroscopy for measurement of the brightness temperature spectrum. In future observations we plan to extend our measurements to all of the submm/mm atmospheric windows, to improve the accuracy of the photometric calibration by eliminating channel fringes from the spectra, and to search for spectral features of H_2S.

5.2. *HCN Abundance*

The unexpected detection of HCN on Jupiter by Tokunaga *et al.* (1981) produced several investigations of its possible sources. Thermochemical models of the time indicated that vertical transport from the deep atmosphere was insufficient to account for the observation (Barshay and Lewis 1978), and several nonequilibrium HCN production mechanisms were therefore proposed: photochemistry of ammonia and methane (Ferris and Chen 1975), hot H-atom chemistry (Lewis and Fegley 1979), photochemistry of ammonia and acetylene (Ferris *et al.* 1992; Ferris and Ishikawa 1988; Kaye and Strobel 1983), and electrical discharge and thunder shock waves (Podolak and Bar-Nun 1988; Stribling and Miller 1987; Bar-Nun and Podolak 1985). These mechanisms were summarized and evaluated by Lewis and Fegley (1984), who identified NH_3–C_2H_2 photochemistry as the most likely source. Subsequent calculations by Fegley and Prinn (1988) and by Fegley and Lodders (1994), however, indicate that vertical transport is indeed sufficient to account for the observed HCN abundance.

Measurement of the vertical distribution of HCN would constitute a key observational constraint on the possible production mechanisms. Tokunaga *et al.* (1981) did not detect any stratospheric emission cores in their original measurements, but were limited by the spectral resolution afforded by their mid-infrared instrumentation. Lellouch *et al.* (1984b) assessed the observability of HCN at submillimetre and millimetre wavelengths by calculating the disk-averaged brightness temperature spectrum. They used the abundance reported by Tokunaga *et al.* as the nominal value in their calculations, and concluded that stratospheric emission cores should be detectable due to the strength of the HCN rotation lines and the high spectral resolution available at these wavelengths using coherent receivers. Lellouch *et al.* (1984a), however, did not detect emission in the $J = 3 \rightarrow 2$ line of HCN at 266 GHz, and placed an upper limit of 4×10^{-9} on the stratospheric HCN mole fraction.

It is clear from the Jupiter : Sun ratios in Fig. 6 and Fig. 7 that the HCN lines at 265.9 GHz ($J = 3 \rightarrow 2$) and 354.5 GHz ($J = 4 \rightarrow 3$) were not detected in these measurements. Moreover the internal measurement errors are small since these ratios do not require an absolute photometric calibration: the statistical error in the Jupiter : Sun ratio at 354.5 GHz, for example, is only 0.28%. Finally, we have demonstrated agreement between the measured and calculated continuum levels (Section 5.1), and systematic errors which would affect the line and continuum differently are extremely unlikely. We are therefore led to conclude that the HCN abundance is much smaller than originally reported by Tokunaga *et al.* (1981).

Since HCN was not detected, we used our atmospheric model to establish an upper limit for the HCN abundance in the jovian troposphere. The 850-μm Jupiter : Sun ratio was used for this analysis since it was less noisy than the 1100-μm ratio. Five different HCN abundance distributions were considered (Fig. 12): (1) uniform throughout the atmosphere, (2) uniform in the tropopause region defined by temperatures below 130 K, (3) uniform in the troposphere but cut off at the tropopause, (4) uniform in the upper troposphere between the 140 K level and the tropopause, and (5) uniform in the deep troposphere but limited in the upper troposphere by condensation. The first four of these correspond to distributions A, B, and C of Lellouch *et al.* (1984b) and the original profile used by Tokunaga *et al.* (1981), respectively, none of which included condensation; since condensation should occur in the cold temperatures of the upper troposphere, however, we consider profile 5 to be the most realistic. We defined the upper limit as the mole fraction which produced a line : continuum ratio equal to the 3σ uncertainty in the nondetection (0.84%). The calculation was carried out for the two cases discussed in Section 5.1, in which the well-mixed ammonia abundance in the deep troposphere was solar and 1.7 times solar. The results are listed in Table 2, and range from 1.7 to 13 times smaller than the Tokunaga *et al.* value. The upper limits for the case of solar NH_3 abundance are shown in Fig. 12.

There are some differences between our calculations and those of Lellouch *et al.* (1984b). In the case of the uniform profile with solar NH_3, for example, the statistical uncertainty in our nondetection is 57 times smaller than the line depth calculated by Lellouch *et al.* The factor of 3 in our calculation of the upper limit reduces this to 19, but our calculated upper limit is only 13 times smaller than the Tokunaga *et al.* (1981) value. This mismatch arises for two reasons. First, Lellouch *et al.* used a pressure-broadened line width at 1 atm of 2.25 GHz, adopted in the absence of any other information from the measurement by Varanasi (1972) of the H_2-broadened widths of

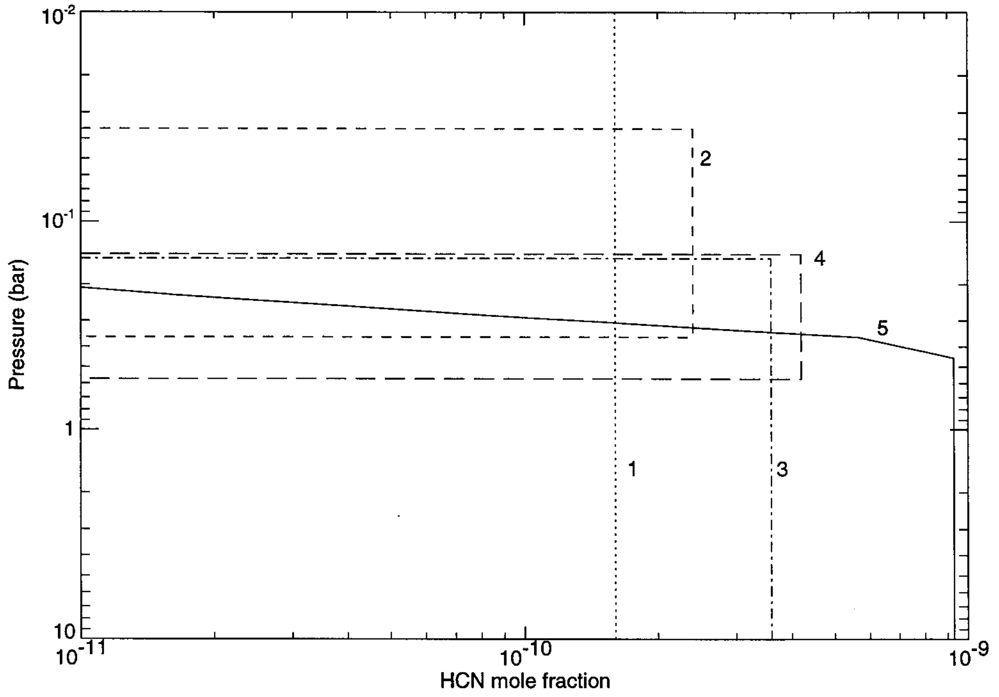

FIG. 12. HCN upper limits for the five different vertical distributions considered in the text: (1) uniform; (2) tropopause region; (3) troposphere; (4) upper troposphere; (5) condensation. The upper limits shown are for the solar NH_3 model.

several rotation–vibration lines in the ν_2 band of NH_3. Since that time, Rohart *et al.* (1987) have calculated the H_2- and He-broadened line widths and their temperature dependences for the first four rotational lines of HCN; their result for the $J = 4 \rightarrow 3$ line is roughly twice the width used by Lellouch *et al.* Second, Lellouch *et al.* integrated over the visible hemisphere of the planet in their model, which reduces the calculated line : continuum ratio; limb darkening is negligible in the present case since the planetary disk was resolved by the JCMT beam.

Our nondetection of HCN (Davis *et al.* 1994) and the establishment of upper limits smaller than the amount originally reported by Tokunaga *et al.* (Davis *et al.* 1995) are consistent with recent results by other workers. Bézard *et al.* (1995) attempted to repeat Tokunaga's original measurement at 13.5 μm but did not detect any features attributable to HCN. They argued that the claimed detection by Tokunaga *et al.* was questionable, and established upper limits of 1×10^{-9} for HCN distributed uniformly throughout the troposphere (our profile 3) and 1.2×10^{-8} for the HCN abundance limited by condensation (our profile 5). Our corresponding upper limits (Table 2) are smaller than these because of the lower noise level in our measurements and the strength of the submillimetre rotational transitions. Weisstein and Serabyn (1996) have also reported nondetection of several HCN rotational lines, and used the $J = 10–9$ transition at 886 GHz to derive upper limits of 3×10^{-10} for HCN distributed uniformly throughout the atmosphere (our profile 1) and 2×10^{-9} for the HCN abundance limited by condensation (our profile 5). Our upper limits are also smaller than these despite our use of a weaker line since Weisstein and Serabyn recorded only eight interferograms. We conclude that our nondetection is consistent with other measurements and that our upper limits are the most restrictive yet reported.

TABLE 2
HCN Upper Limit Mole Fractions

Profile	Distribution	Solar NH_3	$1.7 \times$ solar NH_3
1	uniform	1.4×10^{-10}	1.6×10^{-10}
2	tropopause region	2.2×10^{-10}	2.4×10^{-10}
3	troposphere	3.1×10^{-10}	3.6×10^{-10}
4	upper troposphere	3.8×10^{-10}	4.2×10^{-10}
5	condensation	6.8×10^{-10}	9.3×10^{-10}

5.3. PH_3 $J = 1 \rightarrow 0$ *Line*

Phosphine has been observed in Jupiter in the infrared region from the ground (Tokunaga *et al.* 1979) and from Voyager (Kunde *et al.* 1982; Drossart *et al.* 1982), and recently also at sub-mm wavelengths (Weisstein and Serabyn 1996). As part of their investigation of HCN, Lellouch

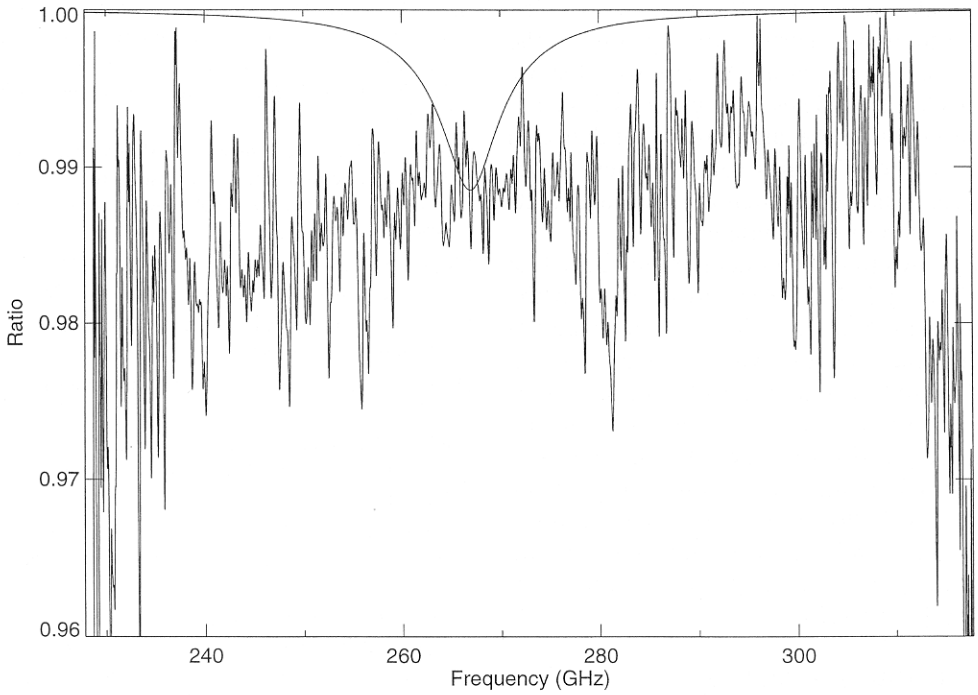

FIG. 13. The smooth curve represents the calculated PH_3 absorption profile at 267 GHz. The noisy curve is one minus the relative noise level in the 1100-μm Jupiter : Sun ratio.

et al. (1984b) modeled the PH_3 absorption feature at 266.9 GHz for various HCN abundances (Fig. 5 of their paper). In the case with no HCN, they obtained a line : continuum ratio of ~13%. This feature is clearly not present in the measured Jupiter : Sun ratio (Fig. 7). The statistical error in this ratio is 1–2% despite the poor atmospheric conditions; for comparison, Weisstein and Serabyn also reported nondetection of this line with 9% uncertainty using a nonpolarizing FTS on the CSO (1994).

We therefore modelled this PH_3 absorption line, following the method described above for HCN. The phosphine vertical distribution derived by Kunde *et al.* (1982) from Voyager measurements in the North Equatorial Belt was adopted; this profile agrees with the recent submillimetre detection by Weisstein and Serabyn (1996) and should also be valid in cloudy regions since PH_3 is not condensable. The calculated line : continuum ratio is shown in Fig. 13. It is immediately apparent that the absorption feature is much shallower than calculated by Lellouch *et al.* (1984b), for two reasons: first, we used the line width value measured by Pickett *et al.* (1981), which is again roughly twice the value used by Lellouch *et al.*; and second, as for HCN, the planet was resolved by the JCMT beam.

Also shown in Fig. 13 is the statistical error in the Jupiter : Sun ratio. It is clear that the PH_3 line was only marginally detectable under the inferior atmospheric conditions which pertained during the run in 1994 May since the calculated line depth is comparable to the noise level. The nondetection is unambiguous if the 3σ criterion is adopted as for HCN. We conclude that the nondetection is not inconsistent with the phosphine profile derived by Kunde *et al.* (1982).

6. CONCLUSIONS

We have measured the Jupiter : Sun brightness ratio in the 850-μm atmospheric window for the first time, and we have also obtained spectra of Jupiter and the Sun in the 1100-μm window. The spectral resolution in both cases was 125 MHz. Three results were obtained.

First, the absorption features due to the rotational lines of HCN at 266 and 354 GHz were not detected. We have established a set of upper limits for HCN in the jovian atmosphere which are between 1.7 and 13 times smaller than the value originally measured by Tokunaga *et al.* (1981), depending on the NH_3 abundance and the assumed HCN distribution profile. This non-detection is supported by independent non-detections by Bézard *et al.* (1995) and by Weisstein and Serabyn (1996).

Second, the continuum brightness temperature at 850 μm is in agreement with a previous whole-disk photometric measurement in this window by Griffin *et al.* (1986). The Griffin *et al.* brightness temperature was corrected for the smaller beam size in the present measurement using a radiative transfer model to facilitate the comparison. The error bars in the continuum spectrum are large due to the uncertainty in the solar temperature at this wavelength. If the opacities of cloud particles and gaseous H_2S are neglected, then we estimate the ammonia abundance in the 1–2 bar region to be 1.7 times solar. If these other opacities are significant, however, then the measurements do not constrain the ammonia abundance.

Finally, we have shown that the nondetection of the first rotational line of PH_3 at 267 GHz is consistent with the previously measured distribution, with current values of the spectroscopic parameters, and with the noise level in the measurements caused by poor atmospheric conditions.

We plan to improve upon these measurements in the near future with the acquisition of a new ^{3}He dual-polarization detector system. Elimination of channel fringes from the measured spectra will allow more accurate continuum calibration against Mars, and enhanced sensitivity should (atmospheric conditions permitting) produce more stringent upper limits on jovian HCN.

ACKNOWLEDGMENTS

The authors thank A. Marten for helpful advice on the radiative transfer model used in this work and P. G. J. Irwin for providing data from the GEISA compilation. It is also a pleasure to thank the technical staff of the JCMT for their support during these observing runs. This research was funded by grants from NSERC and NRC, Canada (GRD, DAN, TAC), and from PPARC, UK (MJG). The James Clerk Maxwell Telescope is operated by the Joint Astronomy Centre on behalf of the Particle Physics and Astronomy Research Council of the United Kingdom, the Netherlands Organization for Scientific Research, and the National Research Council of Canada.

REFERENCES

Bar-Nun, A., and M. Podolak 1985. The contribution by thunderstorms to the abundances of CO, C_2H_2, and HCN on Jupiter. *Icarus* **64,** 112–124.

Barshay, S. S., and J. S. Lewis 1978. Chemical structure of the deep atmosphere of Jupiter. *Icarus* **33,** 593–611.

Ben-Reuven, A. 1966. Impact broadening of microwave spectra. *Phys. Rev.* **145,** 7–22.

Berge, G. L., and S. Gulkis 1976. Earth-based radio observations of Jupiter: Millimeter to meter wavelengths. In *Jupiter* (T. Gehrels, Ed.), pp. 621–692. Univ. of Arizona Press, Tucson.

Bézard, B., A. Marten, J. P. Baluteau, D. Gautier, J. M. Flaud, and C. Camy-Peyret 1983. On the detectability of H_2S in Jupiter. *Icarus* **55,** 259–271.

Bézard, B., D. Gautier, and A. Marten 1986. Detectability of HD and nonequilibrium species in the upper atmospheres of the giant planets from their submillimeter spectrum. *Astron. Astrophys.* **161,** 387–402.

Bézard, B,, C. Griffith, J. Lacy, and T. Owen 1995. Non-detection of hydrogen cyanide on Jupiter. *Icarus* **118,** 384–391.

Carlson, B. E., A. A. Lacis, and W. B. Rossow 1993. Tropospheric gas composition and cloud structure of the jovian north equatorial belt. *J. Geophys. Res.* **98,** 5251–5290.

Clark, T. A., D. A. Naylor, G. J. Tompkins, and W. D. Duncan 1992. Extension of the solar limb at submillimeter and millimeter wavelengths. *Solar Phys.* **140,** 393–396.

Clark, T. A., D. A. Naylor, and G. R. Davis 1994. Detection of the HI $n = 20$–19 transition in emission at the solar limb using a polarizing FT spectrometer. In *IR Tools for Solar Astrophysics: What's Next? Proceedings of the National Solar Observatory 15th Summer Workshop*, pp. 139–144.

Clough, S. A., F. X. Kneizys, E. P. Shettle, and G. P. Anderson 1986. Atmospheric radiance and transmittance: FASCOD2. In *Proceedings of the 6th Conference on Atmospheric Radiation, Williamsburg, May 1986*, pp. 141–144.

Clough, S. A., F. X. Kneizys, and R. W. Davies 1989. Line shape and the water vapor continuum. *Atmos. Res.* **23,** 229–241.

Cohen, E. R., L. Frommhold, and G. Birnbaum 1982. Analysis of the far infrared H_2–He spectrum. *J. Chem. Phys.* **77,** 4933–4941.

Davis, G. R. 1993. The far infrared continuum absorption of water vapour. *J. Quant. Spectros. Radiat. Transfer* **50,** 673–694.

Davis, G. R., D. A. Naylor, M. J. Griffin, W. S. Holland, and T. A. Clark 1994. The non-detection of HCN on Jupiter. *Bull. Am. Astron. Soc.* **26,** 1549.

Davis, G. R., D. A. Naylor, M. J. Griffin, T. A. Clark, and W. S. Holland 1995. The abundance of HCN on Jupiter. *Bull. Am. Astron. Soc.* **27,** 1138–1139.

de Pater, I., and S. T. Massie 1985. Models of the millimeter–centimeter spectra of the giant planets. *Icarus* **62,** 143–171.

Dickerson, R. E. 1978. Chemical evolution and the origin of life. *Sci. Am.* **239**(3), 70–86.

Dore, P., L. Nencini, and G. Birnbaum 1983. Far infrared absorption in normal H_2 from 77 to 298 K. *J. Quant. Spectrosc. Radiat. Transfer* **30,** 245–253.

Drossart, P., T. Encrenaz, V. Kunde, R. A. Hanel, and M. Combes 1982. An estimate of the PH_3, CH_3D, and GeH_4 abundances on Jupiter from the Voyager IRIS data at 4.5 μm. *Icarus* **49,** 416–426.

Duncan, W. D., E. I. Robson, P. A. R. Ade, M. J. Griffin, and G. Sandell 1990. A millimetre/submillimetre common user photometer for the James Clerk Maxwell Telescope. *Mon. Not. R. Astron. Soc.* **243,** 126–132.

Falchi, A., R. Falciani, and P. Mauas 1994. Infrared and submillimeter diagnostics of activity and flares. In *Infrared Solar Physics. Proceedings, IAU Symposium*, Vol. 154, pp. 113–123.

Fegley, B., and K. Lodders 1994. Chemical models of the deep atmospheres of Jupiter and Saturn. *Icarus* **110,** 117–154.

Fegley, B., and R. G. Prinn 1988. The predicted abundances of deuterium-bearing gases in the atmospheres of Jupiter and Saturn. *Astrophys. J.* **326,** 490–508.

Ferris, J. P., R. R. Jacobson, and J. C. Guillemin 1992. The photolysis of NH_3 in the presence of substituted acetylenes: A possible source of oligomers and HCN on Jupiter. *Icarus* **95,** 54–59.

Ferris, J. P., and C. T. Chen 1975. Photosynthesis of organic compounds in the atmosphere of Jupiter. *Nature* **258,** 587–588.

Ferris, J. P., and W. J. Hagan 1984. HCN and chemical evolution: The possible role of cyano compounds in prebiotic synthesis. *Tetrahedron* **40,** 1093–1120.

Ferris, J. P., and Y. Ishikawa 1988. Formation of HCN and acetylene oligomers by photolysis of ammonia in the presence of acetylene: Applications to the atmospheric chemistry of jupiter. *J. Am. Chem. Soc.* **110,** 4306–4312.

Gautier, D., B. Conrath, M. Flasar, R. A. Hanel, V. Kunde, A. Chédin, and N. A. Scott 1981. The helium abundance of Jupiter from Voyager. *J. Geophys. Res.* **86,** 8713–8720.

Griffin, M. J., P. A. R. Ade, G. S. Orton, E. I. Robson, W. K. Gear,

I. G. Nolt, and J. V. Radostitz 1986. Submillimeter and millimeter observations of Jupiter. *Icarus* **65,** 244–256.

Griffin, M. J., and W. S. Holland 1988. The influence of background power on the performance of an ideal bolometer. *Int. J. Infrared Millimeter Waves* **9,** 861–875.

Griffin, M. J., and G. S. Orton 1993. The near-millimeter brightness temperature spectra of Uranus and Neptune. *Icarus* **105,** 537–547.

R. A. Hanel, Conrath, B., Jennings, D. E., and Samuelson, R. E. 1992. *Exploration of the Solar System by Infrared Remote Sensing*, Cambridge Univ. Press, Cambridge, UK.

Holland, W. S., P. A. R. Ade, M. J. Griffin, I. D. Hepburn, D. G. Vickers, C. R. Cunningham, W. K. Gear, P. R. Hastings, W. D. Duncan, T. E. C. Baillie, E. E. Haller, and J. Beeman 1996. 100 mK bolometers for the submillimetre common-user bolometer array. I. Design and construction. *Int. J. Infrared Millimeter Waves* **17,** 669–692.

Husson, N., B. Bonnet, N. A. Scott, and A. Chédin 1992. Management and study of spectroscopic information: The GEISA program. *J. Quant. Spectrosc. Radiat. Transfer* **48,** 509–518.

Jacquinot, P. 1960. New developments in interference spectroscopy. *Rep. Prog. Phys.* **23,** 267–312.

Joiner, J., P. G. Steffes, and K. S. Noll 1992. Search for sulfur (H_2S) on Jupiter at millimeter wavelengths. *IEEE Trans. Microwave Theory Techniques* **MTT-40,** 1101–1108.

Joiner, J., and P. G. Steffes 1991. Modeling Jupiter's millimeter wave emission utilizing laboratory measurements of ammonia (NH_3) opacity. *J. Geophys. Res.* **96,** 17,463–17,470.

Kaye, J. A., and D. F. Strobel 1983. HCN formation on Jupiter: The coupled photochemistry of ammonia and acetylene. *Icarus* **54,** 417–433.

Kunde, V., R. A. Hanel, W. Maguire, D. Gautier, J. P. Baluteau, A. Marten, A. Chédin, N. Husson, and N. A. Scott 1982. The tropospheric gas composition of Jupiter's north equatorial belt (NH_3, PH_3, CH_3D, GeH_4, H_2O) and the jovian D/H isotopic ratio. *Astrophys. J.* **263,** 443–467.

Lellouch, E., M. Combes, and T. Encrenaz 1984a. Microwave observations of Jupiter and Saturn. *Astron. Astrophys.* **140,** 216–219.

Lellouch, E., T. Encrenaz, M. Combes, and P. Drossart 1984b. The observability of HCN on Jupiter in the millimeter range. *Astron. Astrophys.* **135,** 365–370.

Lewis, J. S., and B. Fegley 1979. Hot-atom synthesis of organic compounds on Jupiter. *Astrophys. J.* **232,** L135–L137.

Lewis, J. S., and B. Fegley 1984. Vertical distribution of disequilibrium species in Jupiter's troposphere. *Space Sci. Rev.* **39,** 163–192.

Marten, A., R. Courtin, D. Gautier, and A. Lacombe 1980. Ammonia vertical density profiles in Jupiter and Saturn from their radio electric and infrared emissivities. *Icarus* **41,** 410–422.

Matthews, H. E. 1995. The James Clerk Maxwell Telescope: A guide for the prospective user. Available from the JCMT. See: http://www.jach.hawaii.edu/JCMT/apply.html.

National Oceanic and Atmospheric Administration 1976. *U.S. Standard Atmosphere, 1976.* U.S. Government Printing Office, Washington, DC.

Naylor, D. A., A. A. Schultz, and T. A. Clark 1988. Eliminating channel spectra in Fourier transform spectroscopy. *Appl. Opt.* **27,** 2603–2607.

Naylor, D. A., T. A. Clark, A. A. Schultz, and G. R. Davis 1991. Atmospheric transmission at submillimetre wavelengths from Mauna Kea. *Mon. Not. R. Astr. Soc.* **251,** 199–202.

Naylor, D. A., T. A. Clark, G. R. Davis, W. D. Duncan, and G. J. Tompkins 1993. Broad-band spectroscopy with the James Clerk Maxwell Telescope using a polarizing Fourier transform spectrometer. *Mon. Not. R. Astr. Soc.* **260,** 875–882.

Naylor, D. A., G. R. Davis, M. J. Griffin, T. A. Clark, D. Gautier, and A. Marten 1994a. Broad-band spectroscopic detection of the CO J = 3–2 tropospheric absorption in the atmosphere of Neptune. *Astron. Astrophys.* **291,** L51–L53.

Naylor, D. A., G. J. Tompkins, T. A. Clark, and G. R. Davis 1994b. Polarizing Fourier transform spectrometer for astronomical spectroscopy at submillimeter and mid-infrared wavelengths. In *Instrumentation in Astronomy VIII*, Proc. SPI-E, Vol. 2198, pp. 703–714.

Pickett, H. M., R. L. Poynter, and E. A. Cohen 1981. Pressure broadening of phosphine by hydrogen and helium. *J. Quant. Spectrosc. Radiat. Transfer* **26,** 197–198.

Pickett, H. M., R. L. Poynter, and E. A. Cohen 1995. Submillimeter, millimeter and microwave spectral line catalog. *Available by* anonymous FTP from spec.jpl.nasa.gov.

Podolak, M., and A. Bar-Nun 1988. Moist convection and the abundances of lightning-produced CO, C_2H_2, and HCN on Jupiter. *Icarus* **75,** 566–570.

Rohart, F., D. Derozier, and J. Legrand 1987. Foreign gas relaxation of the $J = 0 \rightarrow 1$ transition of $HC^{15}N$. A study of the temperature dependence by coherent transients. *J. Chem. Phys.* **87,** 5794–5803.

Rothman, L. S., R. R. Gamache, A. Goldman, L. R. Brown, R. A. Toth, H. M. Pickett, R. L. Poynter, J. M. Flaud, C. Camy-Peyret, A. Barbe, N. Husson, C. P. Rinsland, and M. A. H. Smith 1987. The HITRAN database: 1986 edition. *Appl. Opt.* **26,** 4058–4097.

Rothman, L. S., R. R. Gamache, R. H. Tipping, C. P. Rinsland, M. A. H. Smith, D. C. Benner, D. M. Devi, J. M. Flaud, C. Camy-Peyret, A. Perrin, A. Goldman, S. T. Massie, L. R. Brown, and R. A. Toth 1992. The HITRAN molecular database: Editions of 1991 and 1992. *J. Quant. Spectrosc. Radiat. Transfer* **48,** 469–507.

Ruze, J. 1966. Antenna tolerance theory—A review. *Proc. IEEE* **54,** 633–640.

Sagan, C., and S. L. Miller 1960. Molecular synthesis in simulated reducing planetary atmospheres. *Astron. J.* **65,** 499.

Steffes, P. G., and J. M. Jenkins 1987. Laboratory measurements of the microwave opacity of gaseous ammonia (NH_3) under simulated conditions for the jovian atmosphere. *Icarus* **72,** 35–47.

Stribling, R., and S. L. Miller 1987. Electric discharge synthesis of HCN in simulated jovian atmospheres. *Icarus* **72,** 48–52.

Tokunaga, A. T., R. F. Knacke, S. T. Ridgway, and L. Wallace 1979. High-resolution spectra of Jupiter in the 744–980 inverse centimeter spectral range. *Astrophys. J.* **232,** 603–615.

Tokunaga, A. T., S. C. Beck, T. R. Geballe, J. H. Lacy, and E. Serabyn 1981. The detection of HCN on Jupiter. *Icarus* **48,** 283–289.

Varanasi, P. 1972. Shapes and widths of ammonia lines collision-broadened by hydrogen. *J. Quant. Spectrosc. Radiat. Transfer* **12,** 1283–1289.

Wallace, L. 1980. The structure of the Uranus atmosphere. *Icarus* **43,** 231–259.

Weisstein, E. W., and E. Serabyn 1994. Detection of the 267 GHz J = 1–0 rotational transition of PH_3 in Saturn with a new Fourier transform spectrometer. *Icarus* **109,** 367–381.

Weisstein, E. W., and E. Serabyn 1966. Submillimeter line search in Jupiter and Saturn. *Icarus* **123,** 23–36.